Radiation Physics and Chemistry 95 (2014) 73–77

Contents lists available at ScienceDirect

Radiation Physics and Chemistry

journal homepage: www.elsevier.com/locate/radphyschem

High accuracy energy determination and calibration of synchrotron radiation by powder diffraction

L.J. Tantau [a], M.T. Islam [a,b], A.T. Payne [a], C.Q. Tran [c], M.H. Cheah [d], S.P. Best [b], C.T. Chantler [a,*]

[a] School of Physics, The University of Melbourne, Victoria 3010, Australia
[b] School of Chemistry, The University of Melbourne, Victoria 3010, Australia
[c] School of Physics, La Trobe University, Victoria 3086, Australia
[d] UMCiL, Department of Chemistry, University of Malaya, Malaysia

HIGHLIGHTS

- Energy calibration in synchrotron environments where hysteresis is common.
- About 0.1 eV accuracies for a wide range of energy.
- Consecutive runs with the same monochromator and detuning can yield 10–20 sigma discrepancies.
- Offset errors can be critical for comparison to theory and for XANES interpretation.
- Slope errors and offset are significant for XAFS bond lengths and interatomic distances.

ARTICLE INFO

Article history:
Received 29 September 2012
Accepted 20 January 2013
Available online 4 February 2013

Keywords:
Energy calibration
X-ray measurement
Powder diffraction
XAFS beamlines

ABSTRACT

Powder diffraction patterns of standard reference material LaB_6 (660a) have been used to determine the energy of a synchrotron beam across the range 7–12 keV with typical uncertainties of 0.1 eV. Diffraction peaks were recorded on X-ray image plates over a broad range of diffracting angles. Multiple systematic errors were corrected in a robust fitting procedure, providing consistent physical results. We have shown the reliability of this method and observed limitations of reproducibility due to hysteresis by repeated multiple energy calibrations. We report accuracies as low as 13 parts per million (ppm), and demonstrate the need to accurately determine the energy of the X-ray beam during experiments.

1. Introduction

The recent development in fields such as X-ray absorption fine structure (XAFS), X-ray absorption near-edge structure (XANES) and X-ray diffraction (XRD) has relied heavily on the ability to monochromate the broad band of photon energies produced by synchrotron radiation. Energy offsets can occur due to hysteresis of the monochromator motor control and from errors in the reported encoder angle of the monochromator. This becomes problematic in fields that require accurate knowledge of the beam energy.

Previous measurements of K absorption edge energies in transition metals have shown discrepancies of over 6 eV in the literature (Kraft et al., 1996). XAFS oscillations depend on the energy of the incident radiation, hence offsets in energy cause XAFS peaks to shift. More importantly, errors beyond a simple energy offset, of a linear or quadratic or more complex nature, change the dynamical bond lengths and the broadening parameters interpreted by standard XAFS analysis, and any constant offset has a large impact upon XANES interpretation. This is important in fields such as catalysis studies, which employ XAFS and XANES to determine oxidation state of different catalysts (Choi and Lee, 2000). Such analyses often involve detecting small shifts in absorption edge energies, so that energy offsets can lead to inaccurate conclusions.

XRD is a popular method for determining crystal structures. Since the angular location of diffraction peaks depends on the energy of the incident radiation, errors in the monochromator energy reading can produce large offsets in Bragg diffraction peak locations. The use of SRM's to determine photon energies is a common procedure, allowing accurate calibration of the incident beam in order to obtain accurate data (Fleming et al., 2003).

Our group has previously shown discrepancies between standard reference materials (SRMs) LaB_6 (660) and Si (640b) (Chantler et al., 2004) and calibrated the relative lattice spacing

* Corresponding author. Tel.: +61 3 83445437; fax: +61 3 93474783.
E-mail address: chantler@unimelb.edu.au (C.T. Chantler).

0969-806X/$ - see front matter © 2013 Elsevier Ltd. All rights reserved.
http://dx.doi.org/10.1016/j.radphyschem.2013.01.040

through analysis of the physical broadening processes affecting peak profiles (Chantler et al., 2007). This work follows on from the developments by our group in the analysis of diffraction peaks (Rae et al., 2006).

Using SRM LaB_6 (660a) with a well known lattice parameter, we have collected and analysed powder diffraction patterns, which have consequently been used to correct for a systematic shift in the monochromator energy reading. This permits accurate calibration of the beam energy over a broad range of energies. The importance of accurate beam calibration has been demonstrated and a range of applications is discussed.

2. Experimental details

The powder diffraction patterns were recorded on X-ray image plates, mounted on the perimeter of the powder diffractometer BigDiff (Barnea et al., 1992), employing a Debye–Scherrer camera setup. BigDiff's large radius (573 mm) corresponds to 1 cm per degree and permits high resolution profiles to be obtained. Radioactive fiducial markers located at precise locations around the perimeter of BigDiff allow angular positions on the image plates to be calibrated. Full powder patterns are obtained in a relatively short time, permitting simultaneous analysis of multiple systematic errors (Rae et al., 2006).

The LaB_6 powder sample was placed in a capillary with an outer diameter (OD) of 300 μm, which was then attached to one of the eight goniometer heads located in the centre of BigDiff (Creagh et al., 1998). The powder sample was spun at a rate of 60–100 rpm to ensure that all random crystal orientations were averaged over to obtain a full, accurate powder pattern. The diffractometer is evacuated to reduce scattering in the chamber.

Fig. 1 shows 17 powder patterns recorded on a single image plate. Bright black spots at the bottom of the image plate indicate radioactive fiducial markers. Diffraction peaks were collected for five separate experimental runs at regular energy intervals. Four X-ray imaging plates were used for each run, corresponding to an approximate angular region of $-135^\circ < 2\theta < 45^\circ$ for the majority of the data. Fig. 2 illustrates the Bragg peaks and amplitudes across this angular region. The spectrum has minimal background noise permitting accurate peak position determination via a robust fitting procedure.

The capillary holding the powder sample is manually aligned to the beam, so the sample will likely be offset from the diffractometer axis. This eccentricity of the powder sample is described by the parameters δ_y and δ_z, the vertical and horizontal eccentricity, respectively. A similar system comes from the uncertainty in the image plate angular locations, such that each image plate is considered to have a constant angular offset of $\delta\theta_{p_i}$ for the ith image plate. These offsets and how they affect the powder pattern are shown in Fig. 3.

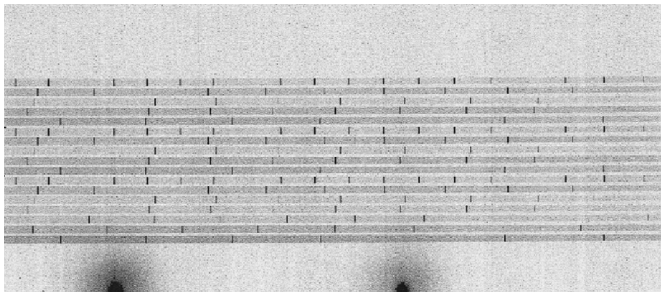

Fig. 1. Powder diffraction patterns recorded on a single image plate, covering an angular region of approximately 40°. The two dark spots at the bottom of the image are the radioactive fiducial markers.

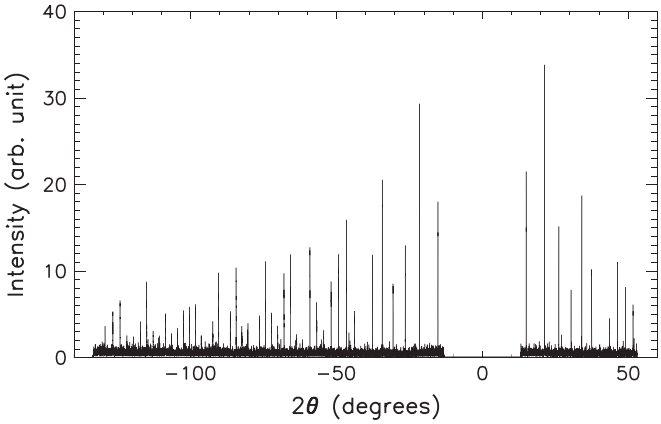

Fig. 2. A typical LaB_6 powder pattern recorded across four image plates, at a nominal energy of 11.3 keV.

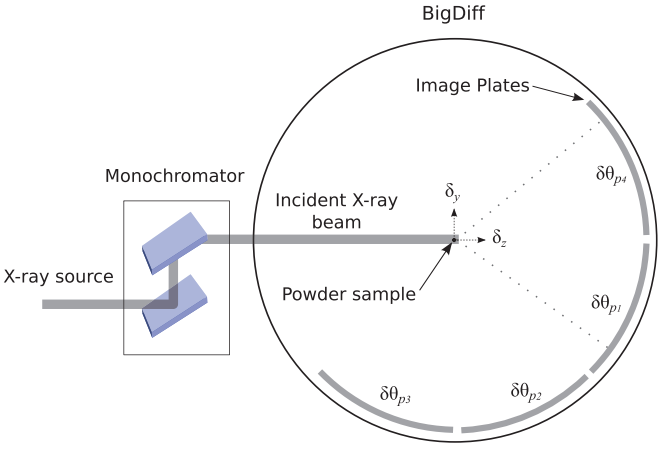

Fig. 3. Schematic of BigDiff, showing the image plate locations and the effect of different offsets such as each individual plate offsets $\delta\theta_{p_i}$ and the sample eccentricity δ_y and δ_z.

The Debye–Scherrer camera setup, illustrated in Fig. 1, allows for multiple powder patterns to be recorded on a single image plate and ensures that powder diffraction pattern measurements are not time consuming. In the energy range considered, exposures of the LaB_6 powder sample in a 300 μm OD capillary typically took 5–10 min depending on the specific energy.

After an experimental run was finished, the image plates were digitised using the Fujifilm BAS2500 image plate reader. Once digitised, the images were then read by the PPDA program, which determines the intensity along a particular diffraction pattern as a function of the diffraction angle 2θ. The angular positions are calibrated by fitting a Gaussian to the recorded fiducial markers.

3. Fitting procedure

A robust peak finding algorithm was applied to detect and locate numerous Bragg peaks. This was subject to two possible problems: cases where Bragg peaks were not detected by the algorithm and cases where spurious peaks were mistakenly detected. Spurious peaks caused incorrect *hkl* indices to be assigned. A filtering process, based on the shape and quality of the peak, was implemented to recognise and discard weak local peaks which were not Bragg reflections. As the powder sample may be approximated as a slit source, each diffraction peak profile

was fitted with a Lorentzian convolved with a slit on a quadratic background.

Bragg peaks were fitted with typical χ_r^2 values between $1<\chi_r^2<10$. For some particular subsets of the data, χ_r^2 was consistently less than one, suggesting a minor over-estimate of the linearised channel intensity uncertainty. The fitted peaks typically had uncertainties in the range 0.0004–0.003° with occasional outliers of $\approx 0.005°$.

For each energy, fitted Bragg peaks were assigned *hkl* Miller indices in a procedure which minimised deviation from the nominal energy. This allowed for the correct set of *hkl* indices to be determined for all peaks of a particular diffraction pattern in a highly automated procedure.

Fitting the Bragg peak positions involved in several parameters: $\delta\theta_{p_i}$ the angular offset for the ith plate; the vertical displacement δ_y, and the horizontal displacement δ_z of the diffracting region of the sample and capillary from the centre of the chamber and image plate axis. For small displacements, these correspond to angular offsets

$$\delta\theta_y = \frac{\delta_y}{R}\cos 2\theta \quad \text{and} \quad \delta\theta_z = \frac{\delta_z}{R}\sin 2\theta, \tag{1}$$

where R is the distance from the capillary to the image plates (the radius of the diffraction chamber). As all parameters are fitted simultaneously in the fitting procedure, this form of δ_y and δ_z orthogonalised these parameters and reduces correlation between fitted parameters. The Bragg peak positions and angular offsets of the peaks were fitted to the Bragg equation to determine the calibrated beam energy

$$\sin(\theta+\delta\theta_{p_i}+\delta\theta_y+\delta\theta_z) = \frac{hc}{2dE_{cal}}, \tag{2}$$

where the E_{cal} is the calibrated beam energy (to be determined), and d is the distance between adjacent lattice planes, given by $d=a_0/\sqrt{h^2+k^2+l^2}$, where a_0 is the lattice parameter.

4. Fitting parameters

Peak centroids were fitted to the Bragg equation with the implementation of a Levenberg–Marquardt least squares fitting procedure. To test the robustness of the parameter space with all offsets included, four combinations of fixing and varying δ_z and δ_y were tested in the fitting procedure:

(a) fixed $\delta_z=\delta_y=0$,
(b) $\delta_z=0$ whilst δ_y varied,
(c) $\delta_y=0$ whilst δ_z varied and
(d) both δ_y and δ_z varied.

Allowing δ_y to vary whilst fixing $\delta_z=0$ as in case (b) rarely reduced χ_r^2 compared to case (a), and in some cases increased χ_r^2.

There was no conclusive evidence for a non-zero δ_y value. This experiment covered a relatively low energy range where relatively few diffraction peaks covered the $-45°<2\theta<45°$ diffraction region which is particularly sensitive to δ_y. This is demonstrated in Fig. 4 which shows the 2θ residuals after fitting δ_y only. The discontinuities are due to the peaks residing on different image plates. There is still strong structure in the Bragg peak residuals after fitting. This suggests that there is a significant non-zero δ_z that was not accounted for by the δ_y offset.

Including only the horizontal offset δ_z whilst fixing $\delta_y=0$ as in case (c) however significantly reduced χ_r^2 across the entire energy range when compared to including no offsets as in case (a). χ_r^2 was reduced by up to a factor of 10 by including the δ_z offset.

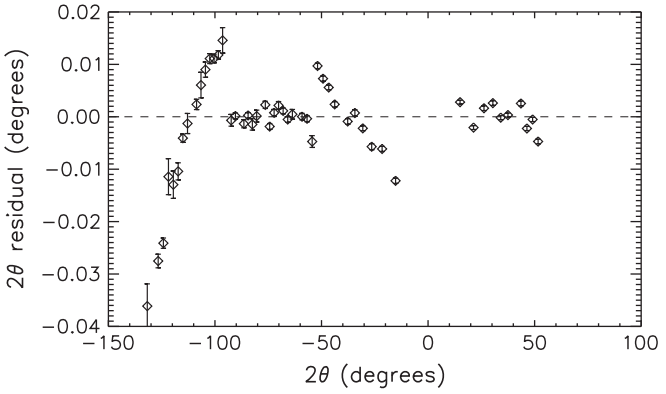

Fig. 4. 2θ residuals for run 2 at 11.3 keV for case (b) after being fitted to the Bragg equation, where $\delta_z=0$ whilst δ_y varied. The residuals are centred about zero as required but clear structure in residuals proves a non-zero δ_z offset.

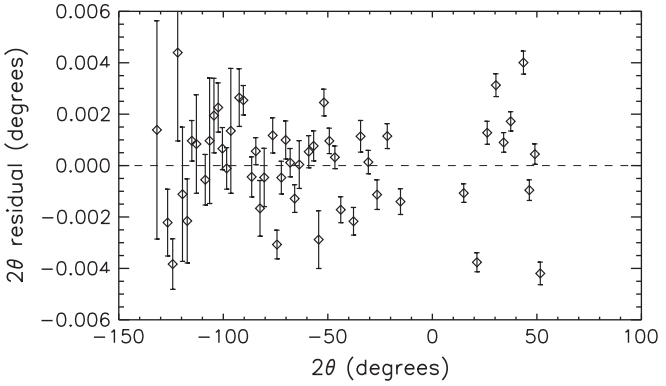

Fig. 5. 2θ residuals for run 2 at 11.3 keV for case (c) after being fitted to the Bragg equation, where $\delta_y=0$ whilst δ_z varied. There is no apparent structure, suggesting appropriate fitting parameters were used and in particular that $\delta_y=0$ within uncertainty.

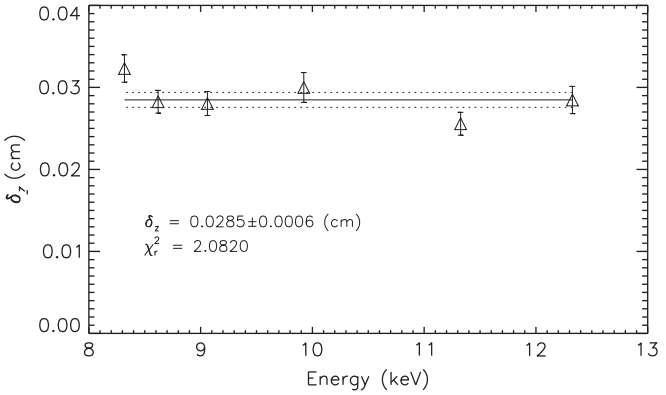

Fig. 6. Horizontal sample offset δ_z plotted against energy for the second run. A constant was fitted to the data, which is plotted as the solid line, including the $\sigma\sqrt{\chi_r^2}$ uncertainty as the dashed line.

Fig. 5 shows no apparent structure in the Bragg peak residuals after being fitted with δ_z, suggesting that this must be accounted for. The dependence of a horizontal sample offset with energy is demonstrated in Fig. 6, showing consistent results for δ_z across the entire range as expected. For this particular run, the horizontal sample misalignment was determined to be $\delta_z=(285\pm6)$ μm.

Finally, case (d), allowing both δ_y and δ_z to vary, generally did not lower χ_r^2 when compared to case (c). This supports the previous finding that varying δ_y did not improve the fits. In case (d), δ_y was consistently determined to be zero to within 1σ.

The function of determined image plate offset with exposure is shown in Fig. 7 for a particular image plate and experimental run. The fitting parameter $\delta\theta_{i=1}$ was consistent across the entire range emphasising the importance of $\delta\theta_i$.

The thermal expansion of the lattice parameter has not been included in this analysis. However it has been shown that the corresponding uncertainty has a negligible effect on final results (Chantler et al., 2004). Other details of analysis and potential systematics are described elsewhere, especially including quadratic functionals, discontinuities and width functional modelling (Chantler et al., 2007; de Jonge et al., 2005; Glover et al., 2008).

5. Individual results

The energy correction is defined as $E_{correction} = E_{cal} - E_{nom}$, where E_{cal} is the calibrated energy, calculated using the outlined procedure and E_{nom} is the nominal beam energy, reported by the monochromator itself. Energy corrections for a particular run are shown in Fig. 8 and fitted with a straight line. The data fit extremely well with final uncertainties down to 0.1 eV near the XAFS region of interest. The 5–10 energy calibrations via powder diffraction were used to correct the nominal values of all energies, which was often around 300 different energies per run. Incidentally, because of the careful optimisation of this experiment, the result is significantly more accurate than previous analyses and literature using this system, which usually had a minimum uncertainty of 1–3 eV.

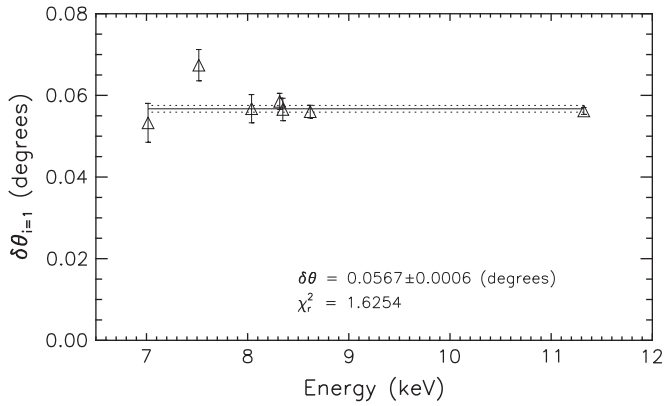

Fig. 7. Plate offset $\delta\theta_{i=1}$ plotted against energy for the final run. The solid line is the weighted mean, including the $\sigma\sqrt{\chi^2_r}$ uncertainty as the dashed line.

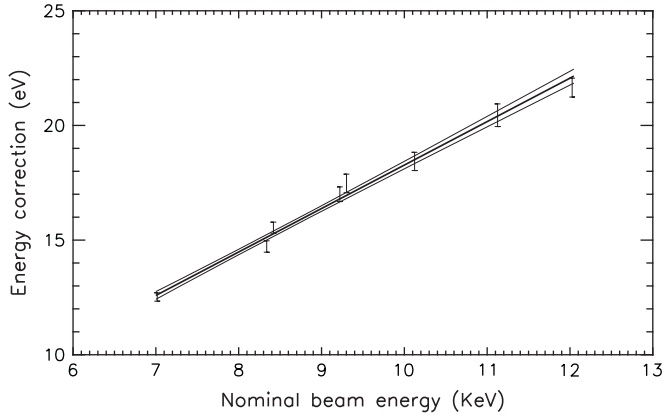

Fig. 8. Correction to the nominal energy of the X-ray beam (run 1). The thick black line represents the fitted line, whilst the thin lines are the $1-\sigma$ uncertainty. Data points are represented by their error bars. The final uncertainty is less than 0.5 eV across the entire range, and down to 0.1 eV in the XAFS region of interest.

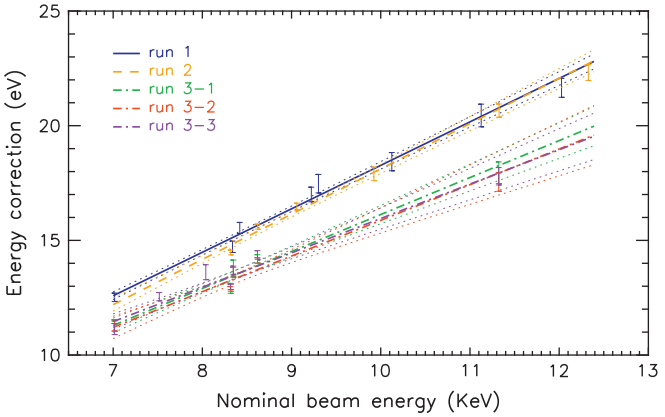

Fig. 9. Correction to the nominal energy of the X-ray beam. Each different colour represents a different experimental runs, with the monochromator being reset after each run. Change three involved three runs using the same set of image plates.

6. Comparison of different runs

Calibration curves were investigated across five separate experimental runs. Each run determined the absorption and fluorescence spectrum of various nickel samples for XAFS calculations. The first two runs were recorded on the separate sets of image plates, whilst the final three calibrations were all recorded on the same set of image plates (without being removed or erased).

The five different coloured lines of Fig. 9 represent different runs during the experiment, where the monochromator angle was reset after each run. Each separate run involved changing energy from 12 to 7 keV with hundreds of intermediary steps. When reset, the monochromator was set to around 15 keV, and gradually reduced to 12 keV where the next run started, to avoid hysteresis of the motor control. Fig. 9 shows that the energy calibration curve for the three runs on change three are highly consistent, to within their $1-\sigma$ error, whilst the first two runs have a slightly larger offset. Runs 1 and 2 have very similar calibration curves, to within their $1-\sigma$ error, but were recorded on different imaging plates.

This discrepancy could be caused by a systematic error in image plate tilt. This was directly investigated and found to have no effect on the results. Output from the PPDA program, designed specifically to read image plates from BigDiff, measures the plate tilt and automatically corrects for this. The tilt correction was generally between $-0.15 < \theta_{tilt} < 0.15$, which is the angle that the diffraction pattern stripe makes to the nominal horizontal.

With the new accuracy reported from the five separate energy calibrations, Fig. 9 indicates that each time the monochromator is reset, whilst under the same experimental conditions, different calibration curves are determined. This is of great importance, as it suggests that the energy offset and slope are unique to each experimental run. Consequently, it suggests that consistent and absolute values for photon energies at a synchrotron source should involve direct calibration functions. However making relatively few direct measurements can yield accuracies of 0.1 eV in regions of interest, whilst not compromising experimental time constraints.

7. Applications

Powder diffraction using SRM's with well known lattice parameters can provide fast and accurate energy calibration over a wide range of energies in X-ray experiments. This can be used to

accurately determine absorption edge energies in XAFS, where fields such as catalysis studies require accurate measurements of this edge energy to determine bonding and coordination properties of different types of catalysts (Meitzner et al., 1988).

This method has also been used to show small discrepancies in the lattice parameter of LaB_6 (SRM660)[1] relative to the lattice parameter of Si (640b) (Chantler et al., 2007). Our group plans to perform similar comparisons for the current series of SRMs, namely LaB_6 (660a) and Si (640d). XRD experiments require precise knowledge of the wavelength of the incident radiation, and hence its energy. Specifically, powder diffraction experiments are able to calibrate energy accurately and in a short period of time.

Many synchrotron experiments depend upon energy calibration in an absolute sense (XANES) or a relative sense (XAFS) especially if available theoretical predictions have an absolute energy axis. Specialised or high-accuracy experiments will also benefit from direct energy calibration to a high level.

8. Conclusion

We have accurately determined the energy of a synchrotron beam by measuring diffraction peaks of SRM LaB_6 (660a) with the powder diffractometer BigDiff. With careful analysis of experimental parameters and systematic errors, this method has proven to be a fast, reliable and accurate way to measure the energy of a beam with final uncertainties down to 0.1 eV or 13 ppm.

The requirement to calibrate the energy of a synchrotron beam for each separate experiment has been demonstrated through analysis of multiple results. This suggests that the error from the angle encoder reading on the monochromator must be taken into account for accurate energy determination and need not be stable even in short term. Accurate energy calibration is crucial in fields such as XAFS, XRD and critical tests of X-ray photoabsorption. Our method provides a consistent and fast way of providing accurate determination of the beam energy.

Acknowledgements

The authors acknowledge the experimental team and local ANBF staff, guidance from Nicholas Rae and the support of the ARC and ASRP with grants for this work.

References

Barnea, Z., Creagh, D.C., Davis, T.J., Garrett, R.F., Janky, S., Stevenson, A.W., Wilkins, S.W., 1992. The Australian diffractometer at the photon factory. Rev. Sci. Instrum. 63, 1069–1072.

Chantler, C.T., Rae, N.A., Tran, C.Q., 2007. Accurate determination and correction of the lattice parameter of LaB_6 (standard reference material 660) relative to that of Si (640b). J. Appl. Crystallogr. 40, 232–240.

Chantler, C.T., Tran, C.Q., Cookson, D.J., 2004. Precise measurement of the lattice spacing of LaB_6 standard powder by the X-ray extended range technique using synchrotron radiation. Phys. Rev. A 69, 042101.

Choi, S.H., Lee, J.S., 2000. XAFS study of tin modification of supported palladium catalyst for 1,3-butadiene hydrogenation in the presence of 1-butene. J. Catal. 193, 176–185.

Creagh, D.C., Foran, G.J., Cookson, D.J., Garrett, R.F., Johnson, F., 1998. An eight-position capillary sample spinning stage for the diffractometer at BL20B at the photon factory. J. Synchrotron Radiat. 5, 823–825.

de Jonge, M.D., Tran, C.Q., Chantler, C.T., Barnea, Z., Dhal, B.B., Cookson, D.J., Lee, W.K., Mashayekhi, A., 2005. Measurement of the X-ray mass attenuation coefficient and determination of the imaginary component of the atomic form factor of molybdenum over the 13.5–41.5-keV energy range. Phys. Rev. A 71 032702/1–16.

Fleming, D.E., Van Riessen, A., Chauvet, M.C., Grover, P.K., Hunter, B., Van Bronswijk, W., Ryall, R.L., 2003. Intracrystalline proteins and urolithiasis: a synchrotron X-ray diffraction study of calcium oxalate monohydrate. J. Bone Miner. Res. 18, 1282–1291.

Glover, J.L., Chantler, C.T., Barnea, Z., Rae, N.A., Tran, C.Q., Creagh, D.C., Paterson, D., Dhal, B.B., 2008. Measurements of the X-ray mass attenuation coefficient and imaginary component of the form factor of copper. Phys. Rev. A 78, 52902.

Kraft, S., Stumpel, J., Becker, P., Kuetgens, U., 1996. High resolution X-ray absorption spectroscopy with absolute energy calibration for the determination of absorption edge energies. Rev. Sci. Instrum. 67, 681–687.

Meitzner, G., Via, G.H., Lytle, F.W., Fung, S.C., Sinfelt, J.H., 1988. Extended X-ray absorption fine structure (EXAFS) studies of platinum–tin catalysts. J. Phys. Chem. 92, 2925–2932.

Rae, N.A., Chantler, C.T., Tran, C.Q., Barnea, Z., 2006. Accurate determination of X-ray energies using powder diffraction. Radiat. Phys. Chem. 75, 2063–2066.

[1] This experiment used LaB_6 (660a), the successor to LaB_6 (660).